Computational and Theoretical Chemistry 1040–1041 (2014) 338–346

Contents lists available at ScienceDirect

Computational and Theoretical Chemistry

journal homepage: www.elsevier.com/locate/comptc

Ground state structures and electronic excitations of biological chromophores at Quantum Monte Carlo/Many Body Green's Function Theory level

Daniele Varsano [a,*], Emanuele Coccia [b], Olivia Pulci [c], Adriano Mosca Conte [c], Leonardo Guidoni [b,*]

[a] S3 Center, CNR Institute of Nanoscience, via Campi 213/A, 41125 Modena, Italy
[b] Dipartimento di Scienze Fisiche e Chimiche, Universitá degli Studi dell'Aquila, via Vetoio, 67100 Coppito, L'Aquila, Italy
[c] ETSF, Dipartimento di Fisica, Universitá di Roma Tor Vergata, Via della Ricerca Scientifica 1, 00133 Rome, Italy

ARTICLE INFO

Article history:
Received 2 February 2014
Received in revised form 6 March 2014
Accepted 6 March 2014
Available online 15 March 2014

Keywords:
Multiscale calculations
Bethe–Salpeter equation
Carotenoids
Rhodopsin
Absorption spectrum

ABSTRACT

The accurate calculation of electronic excited states of large and electronically correlated biological chromophores in their complex protein environment still represents a challenge for quantum chemistry. Two *ab initio* techniques are recently emerging as candidates to correctly tackle this issue: Quantum Monte Carlo (QMC) calculations for the ground state geometry optimization, and Many Body Green's Function Theory (MBGFT) for exited state energies. In the present work we use the Variational Monte Carlo (VMC) to carry out structural optimizations and we present an extension of MBGFT to complex environments, using a Quantum Mechanics/Molecular Mechanics framework. This technique is applied to evaluate the optical properties of the retinal protonated Schiff base (**RPSB**) chromophore in rhodopsin, the protein responsible for dim light vision in the vertebrates. Vertical energies for the bright excitation of **RPSB** calculated solving the Bethe–Salpeter equation in gas phase and in the protein environment correspond to 2.19 eV and 2.58 eV, respectively. These data are in fair agreement with the available experimental findings. The comparison between these excitation energies and that obtained for a gas phase calculation on a retinal geometry obtained in the protein environment (2.03 eV) reveals the essential role of the protein field in the spectral tuning of the molecule. The proposed VMC/MBGFT methodologies can therefore be applied to obtain a reliable *ab initio* evaluation of optical properties of biological chromophores.

1. Introduction

The optical properties of natural pigments play an important role in many biological processes such as the dim light and color vision in the eyes [1], the light-harvesting in photosynthetic organisms [2,3], and the bioluminescence [4] among others. The possibility to predict with high accuracy by first principles the positions and the intensities of the absorption peaks (i.e. the color [5]) of such chromophores in their natural protein environment opens the way to the interpretation of experimental data and to the design of biologically-inspired light-harvesting devices.

Color tuning is usually rationalized in terms of two main aspects: (i) the structural features of chromophore, and (ii) the modifications of the electronic properties (such as ground and excited state densities) due to the interaction with the polar and/or charged residues of the surrounding protein matrix. The interplay between geometry and absorption properties is one of the key ingredients which must be taken into account to tackle the problem of the color tuning of biological chromophores. In particular, many chromophores are characterized by long conjugated carbon chains with a clear bond length alternation (BLA) between single and double bonds which can be significantly influenced by geometrical distortion and field effects. Since the BLA geometrical descriptor has been shown to correlate with the λ_{max} value in the optical absorption [6], the accurate evaluation of the ground state geometry becomes a crucial task. The possibility to use high-level quantum chemistry techniques, with a balanced amount of electronic correlation, is of primary importance for theoretical photochemistry: in the case of linear polyenes, DFT functionals (LDA, GGA, hybrids, long-range corrected hybrids, etc.) offer a wide range of values of the BLA, usually overestimating the correlation along the polyenic chain, whereas the use of Coupled Cluster or

* Corresponding authors.
E-mail addresses: daniele.varsano@nano.cnr.it (D. Varsano), leonardo.guidoni@univaq.it (L. Guidoni).

http://dx.doi.org/10.1016/j.comptc.2014.03.011
2210-271X/

truncated-CI methods is limited to medium-size systems, due to the prohibitive computational costs [7–9].

Quantum Monte Carlo (QMC) methods [10–12] can be considered a valid alternative in quantum chemistry thanks to their specific suitability for massively parallel High Performance Computing facilities. QMC techniques show a good scaling with respect to the system size (N^d, with N the number of electrons and $3 < d < 4$), similar to the DFT one (N^3); the large prefactor in the QMC scaling is drastically reduced by the high parallelism of QMC codes, allowing one to efficiently use thousands of computational cores at the same time [13], and to apply QMC to systems up to ~200/300 electrons, i.e. the valence electrons of organic molecules up to 100 atoms [6]. In addition, a recent implementation of a QMC/MM interface allows us to calculate ground state structures of molecular targets embedded in complex environments [14].

Variational Monte Carlo (VMC) geometry optimization has been so far applied to molecules of biological interest like gas phase retinal models [14,15] and the retinal chromophore in rhodopsin [14]. A very recent work by us [6], reports the VMC structural optimization of the gas phase peridinin carotenoid, together with a systematic analysis of the spectral tuning of the bright excited B_u^+-like state.

Similarly, the calculation of excited state properties of organic dyes or biological pigments represents an open issue for theoreticians: TDDFT [16,17] can be considered in many cases a good compromise between accuracy and computational effort, with a variety of functionals and some specific limitations (for instance, charge-transfer excitations and double excitation character in transitions); on the other hand, multireference (CASSCF [18], CASPT2 [19,20], NEVPT2 [21–23], CISD [24], etc.), parameterized DFT/MRCI [25,26], and single reference (Coupled Cluster [27] derived approaches) methods are very accurate but too much demanding in terms of computational cost for large chemical systems (hundreds of electrons) [28].

Many Body Green's Function Theory (MBGFT) [29] has been widely used in condensed matter physics [29]. MBGFT has been successfully used to describe with high accuracy quasiparticle energies and optical excitations in polyenic chains where TDDFT with local and semilocal approximation dramatically fails [30], but only few applications to molecular problems of (bio) chemical interest are present in literature [6,31–34].

Furthermore, a very recent implementation of MBGFT code efficiently exploits High Performing Computing facilities [35], like the BlueGene architecture. For these reasons VMC and MBGFT represent two promising candidates to investigate the geometrical and optical properties of medium- and large-size protein pigments at high-level of theory. Thanks to the developments of high-performance computing and recent important technical improvements, only in the few last years the two techniques have been applied to chromophores of biological interest. In the case of MBGFT, few chromophores were investigated in gas phase by Ma et al. [31,32]: the GFP, PYP, PSB, and the peridinin carotenoid by some of us [6].

An additional important ingredient is to perform the calculations within a QM/MM scheme, to take into account the effect of the surrounding environment. Such calculations, so far applied only to the case of indole in water solution [36], are presented in this work for a protein chromophore: the widely studied retinal (retinal protonated Schiff base, **RPSB**, Fig. 1) in rhodopsin, comparing our results with the experimental data and other quantum chemistry calculations.

The main goal of this work is to extend this fully *ab initio* computational procedure based on VMC and MBGFT to the calculations of absorption spectra of **RPSB** in situ, through a QM/MM scheme.

The paper is organized as follows: Section 2 shows theory and details on implementation for both QMC and MBGFT methods used in this work; details on calculations are collected in Section 3; in Section 4 our recent VMC/MBGFT results [6] on the gas phase peridinin carotenoid (**PID**) are briefly summarized and the present VMC/MBGFT values for S_1 and S_2 singlet excited state energies of **RPSB** are reported and compared with theoretical and experimental reference values, focusing the attention to the shifts due to the protein environment and to geometrical distortions; finally, we present our conclusions and perspectives for the use of the fully *ab initio* approach to calculate vertical excitations in gas phase and in complex environments, pointing out the possibility to extend the VMC/MBGFT procedure to larger important biological pigments, such as carotenoids and chlorophylls, in their protein environment.

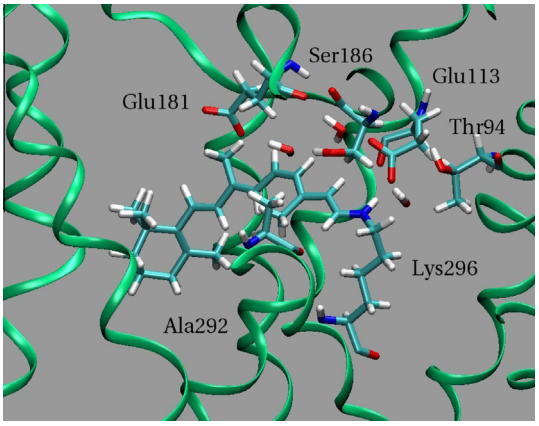

Fig. 1. RPSB in the rhodopsin pocket: the protein residues affecting the S_1 excitation energy are highlighted [37].

2. Theoretical methods

2.1. Quantum Monte Carlo

2.1.1. Variational Monte Carlo

The Variational Monte Carlo (VMC) [11,12] energy E_{VMC} is obtained by searching the minimum of the expectation value of the electronic molecular Hamiltonian H, over a set of variational parameters $\mathbf{p} = \{p_i\}$ of a trial wave function Ψ_T in the electronic coordinate space $\mathbf{x}$, given a specific nuclear configuration $\mathbf{R}$:

$$E_{\mathrm{VMC}} = \min_{\mathbf{p}} E[\Psi_T(\mathbf{x};\mathbf{p},\mathbf{R})], \tag{1}$$

where

$$E[\Psi_T] = \langle H \rangle_{\Psi_T^2} = \frac{\int \Psi_T(\mathbf{x};\mathbf{p},\mathbf{R})\, H\, \Psi_T(\mathbf{x};\mathbf{p},\mathbf{R}) d\mathbf{x}}{\int \Psi_T^2(\mathbf{x};\mathbf{p},\mathbf{R}) d\mathbf{x}}. \tag{2}$$

The integral in Eq. (2) can be written in terms of the *local energy*, defined as $E_L = H\,\Psi_T/\Psi_T$, and of a probability density $\Pi = \frac{|\Psi_T^2|}{\int |\Psi_T^2| d\mathbf{x}}$:

$$E[\Psi_T] = \frac{\int \Psi_T^2(\mathbf{x};\mathbf{p},\mathbf{R}) E_L(\mathbf{x};\mathbf{p},\mathbf{R}) d\mathbf{x}}{\int \Psi_T^2(\mathbf{x};\mathbf{p},\mathbf{R}) d\mathbf{x}}. \tag{3}$$

The integral is then calculated stochastically through a sum over a set of random points $\mathbf{x}$ in the configurational space of the $6N$ electronic Cartesian and spin coordinates, distributed according to Π.

The structural optimization within the VMC scheme implies the simultaneous minimization of the energy functional with respect to the variational parameters $\mathbf{p}$ of Ψ_T and the nuclear coordinates $\mathbf{R}$:

$$E_{\mathrm{VMC}}^{OPT} = \min_{\mathbf{p},\mathbf{R}} E[\mathbf{R};\Psi_T(\mathbf{x};\mathbf{p},\mathbf{R})]. \tag{4}$$

The structural minimum searching is provided by a simple steepest descent method taking into account the random noise. The ionic forces acting along the coordinates $\mathbf{R}$ are defined for each nucleus A as:

$$\mathbf{F}_A(\mathbf{R}) = -\nabla_{\mathbf{R}_A} E_{VMC}(\mathbf{R}, \mathbf{p}(\mathbf{R})). \tag{5}$$

VMC forces for the nucleus A are given by the sum of two terms: the Hellmann–Feynman $\mathbf{F}_A^{H-F}(\mathbf{R}) = -\left\langle \frac{dE_L}{d\mathbf{R}_A} \right\rangle_{\Pi}$ and Pulay $\mathbf{F}_A^{P}(\mathbf{R}) = 2\left\{ \langle E_L \rangle_{\Pi} \left\langle \frac{d\ln|\Psi_T|}{d\mathbf{R}_A} \right\rangle_{\Pi} - \left\langle E_L \frac{d\ln|\Psi_T|}{d\mathbf{R}_A} \right\rangle_{\Pi} \right\}$ terms [10]. Several techniques have been implemented in order to reduce the variance on the ionic forces and to improve the accuracy of the calculation: (i) the so-called Space Warp Coordinate Transformation (SWCT) [38–40], (ii) the use of the reweighting method [41,40,42] at the nodal surface, (iii) the Adjoint Algorithmic Differentiation scheme [39].

In order to study the effect of the protein environment on the chromophore a QMC/MM interface has been implemented in the TurboRVB package [43]. We have followed the approach used in the CPMD code [44,45] to treat the electrostatic coupling between the electronic density of the QMC subsystem and the point charges coming from the classical force field describing the large MM (Molecular Mechanics) subsystem, as explained in the Supporting Information of Ref. [14]. Details on the classical force field and, generally, on the QMC/MM Hamiltonian are given below.

2.1.2. JAGP wave function

The Jastrow Antisymmetrised Geminal Power (JAGP) trial wave function [46–51], is defined as the product between the Antisymmetrised Geminal Power (AGP) and a Jastrow factor $J(\mathbf{r})$

$$\Psi_T(\mathbf{x}) = \Psi_{AGP}(\mathbf{x}) \times J(\mathbf{r}) \tag{6}$$

where $\mathbf{r}$ represents the collective $3N$ electron Cartesian coordinate. The AGP term is intrinsically multiconfigurational [52] while the Jastrow factor J (spin-independent factor to avoid spin contamination) includes dynamical electronic correlation.

For a spin-unpolarized molecular system of N electrons and M nuclei, i.e. $N/2 = N^{\uparrow} = N^{\downarrow}$, the AGP is written as

$$\Psi_{AGP}(\mathbf{x}) = A \prod_{i}^{N/2} \Phi_G(\mathbf{x}_i^{\uparrow}; \mathbf{x}_i^{\downarrow}) \tag{7}$$

where A is the antisymmetrization operator and Φ_G is the Geminal pairing function:

$$\Phi_G(\mathbf{x}_i; \mathbf{x}_j) = \phi_G(\mathbf{r}_i, \mathbf{r}_j) \frac{1}{\sqrt{2}} \left(|\uparrow\rangle_i |\downarrow\rangle_j - |\uparrow\rangle_j |\downarrow\rangle_i \right). \tag{8}$$

The spatial function $\phi_G(\mathbf{r}_i, \mathbf{r}_j)$ is a linear combination of products of atomic orbitals:

$$\phi_G(\mathbf{r}_i, \mathbf{r}_j) = \sum_{A,B}^{M} \sum_{\mu,\nu} \lambda_{\mu_A \nu_B} \psi_{\mu_A}(\mathbf{r}_i) \psi_{\nu_B}(\mathbf{r}_j) \tag{9}$$

where the indexes μ and ν are related to the basis sets centered on the A-th and B-th nuclei.

The Jastrow term J is split into a product of three or four terms $J = J_1 J_2 J_{3/4}$, introducing dynamical correlation and satisfying the electron–electron and electron-nucleus cusp conditions. A detailed explanation of this function is given by Zen et al. in Ref. [42].

2.2. Optical properties by Many Body Green Function Perturbation Theory (MBGFT)

In this section we briefly recall the key ingredients of MBGFT for the calculation of the quasi-particle energies in the GW approximation and for the optical spectra in the Bethe–Salpeter approach and its extension to the QM/MM scheme. A complete overview of MBGFT can be found in Ref. [29] and further details on the QM/MM coupling scheme can be found in Ref. [36].

In practice, the calculation of optical excitations is carried out in a three-step procedure. First, we obtain the ground state electronic properties of the relaxed system, by performing a DFT supercell calculation, within the local density approximation (LDA). Second, the quasi-particle corrections to the LDA eigenvalues are evaluated within the not self-consistent GW approximation for the self-energy operator ($\Sigma = iG^0W^0$), where the LDA wave functions are used as good approximations for the quasiparticle ones. The dynamical screening is treated within the plasmon-pole approximation [53]. Finally, the electron–hole interaction is included by solving the Bethe–Salpeter (BS) equation in the basis set of quasi-electron and quasi-hole states, where the static screening in the direct term is calculated within the random-phase approximation (RPA). The constructed excitonic Hamiltonian is then diagonalized going beyond the Tamm–Dancoff approximation, i.e. including the coupling between resonant and anti resonant part, as it has been shown it cannot be neglected in molecular systems [31,32,54]. Finally from the solution of the BS equation, the absorption spectra are then computed as the imaginary part of the macroscopic dielectric function. In order to include the effects of the protein environment, the quasi-particle equation derived from the Dyson equation for the Green's function in the Lehmann representation [29] has been modified as [36]:

$$\begin{aligned} &\left[-\frac{\hbar^2 \nabla^2}{2m} + U^{QM}(\mathbf{r}) + U^{QM/MM}(\mathbf{r}) + V_H(\mathbf{r}) \right] \phi_j^{QP,QM/MM}(\mathbf{r}) \\ &+ \int d^3\mathbf{r}' \Sigma\left(\mathbf{r}, \mathbf{r}', \varepsilon_j^{QM/MM}\right) \phi_j^{QP,QM/MM}(\mathbf{r}') \\ &= \varepsilon_j^{QP,QM/MM} \phi_j^{QP,QM/MM}(\mathbf{r}). \end{aligned} \tag{10}$$

In this expression U is the external potential, V_H is the Hartree potential, Σ is the electron non-local and energy dependent self-energy operator that takes into account the dynamical screening. $\varepsilon_j^{QP,QM/MM}$ and $\phi_j^{QP,QM/MM}$ are respectively quasi-particle energies and eigenfunctions. Eq. (10) differs from a full-QM equation in the expression of the external potential, that has been split in two contributions: U^{QM} is the external potential induced by the ions of the quantum subsystem, while $U^{QM/MM}$ comes from the electrostatic coupling of the QM part with classical MM, described as point-charges. The MM part is therefore directly included in the fundamental equations for the calculation of the quasi-particle eigenvalues and eigenvectors, and its effect is intrinsically included in the GW method. Actually the quantities used in the GW method are built using eigenvalues $\varepsilon_j^{QM/MM}$ and eigenvectors $\phi_j^{QM/MM}(\mathbf{r})$ coming for a coupled QM/MM calculation.

Similarly the $\phi_j^{QM/MM}(\mathbf{r})$ coming from the coupled QM/MM calculation together with the quasi-particle energies $\varepsilon_j^{QP,QM/MM}$ calculated in the coupled scheme (Eq. (10)) are used to build the effective excitonic two-body Hamiltonian [55] coming from the BS equation.

The absorption spectrum is then calculated by the following:

$$\begin{aligned} \epsilon_M(\omega) = 1 - \lim_{q \to 0} v(\mathbf{q}) \sum_{\lambda,\lambda'} \Bigg[&\sum_{n_1,n_2} \langle n_1 \mid e^{-i\mathbf{q}\cdot\mathbf{r}} \mid n_2 \rangle \times \frac{A_{\lambda}^{(n1,n_2)}}{\omega - E_{\lambda} + i\eta} N_{\lambda,\lambda'}^{-1} \\ &\times \sum_{n_3,n_4} \langle n_4 \mid e^{-i\mathbf{q}\cdot\mathbf{r}} \mid n_3 \rangle A_{\lambda'}^{*(n1,n_2)} (f_{n_3} - f_{n_4}) \Bigg] \end{aligned} \tag{11}$$

where

$$N_{\lambda,\lambda'}^{-1} = \sum_{n_1,n_2} A_{\lambda}^{*(n1,n_2)} A_{\lambda'}^{(n1,n_2)}, \tag{12}$$

and $A_{\lambda}^{(n1,n_2)}$ are the electron–hole amplitudes of the excitation λ, eigenvectors of the excitonic Hamiltonian. We stress here that the main assumption for interfacing a MBGFT approach with a classical region is that the optical properties of the chromophore do not involve the electronic structure of the MM part. Hence, special care has to be devoted to the choice of the two regions. This method is perfectly suited for studying optical properties of protein chromophores whose optical active part is confined to the pigment. The typical size of a biological chromophore is around 100 atoms, that can be treated by MBGFT, while the rest of the protein, including water molecules, are treated by classical MM.

3. Computational details

3.1. Quantum Mechanics/Molecular Mechanics

A QM/MM scheme has been adopted for both the VMC geometry optimization and the MBGFT calculations. VMC structural data for **PID** and **RPSB**, summarized in Figs. 2 and 3, are reported from Refs. [6,14]. For the VMC/MM geometry optimization (only **RPSB**) standard bonded potentials are used in the case at least one QMC atom is involved in the interaction; all the classical atoms are kept fixed. The additional external field interacting with the electronic density $\rho(\mathbf{r})$ has been generated using classical point charges coming from the Amber force field screened at short range to avoid electronic spill-out [44]. The full chromophore is treated at quantum level and one hydrogen link atom is added to saturate the covalent bond with the nitrogen atom of Lys296 [56]. Starting from the chain A of the 1HZX structure [57], a DFT/BLYP annealing of the full system (comprising water and membrane of the biological environment) has been performed; the converged coordinates have then been used for defining the VMC and MM subsystems in the VMC/MM procedure and used as starting point for the VMC/MM optimization. Details on the classical and QM/MM setups are reported in Ref. [14] and references therein.

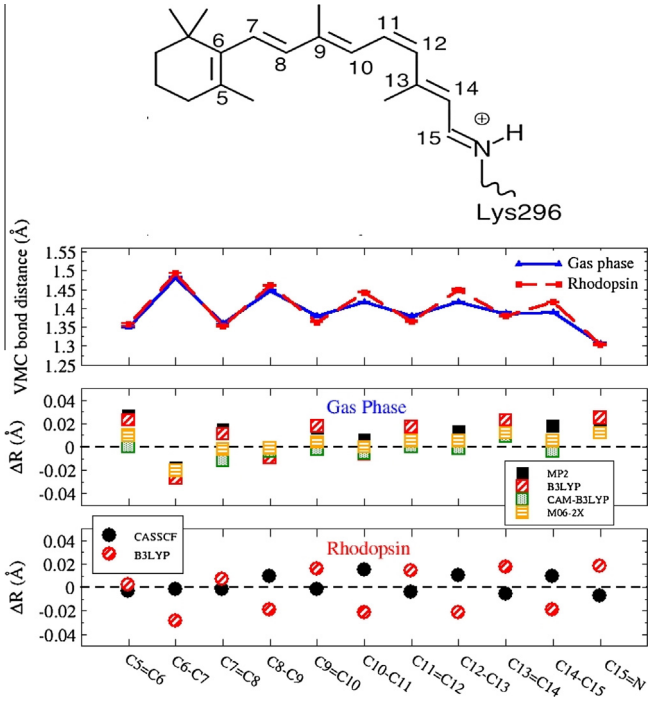

Fig. 3. RPSB: sketch representation of the chromophore, VMC BLA pattern for gas phase and protein-embedded models and differences with respect to literature structures (the references are given by the VMC geometries). The average BLA for the VMC structure is 0.059(3) Å and 0.088(3) Å, for gas phase and rhodopsin models, respectively. The C_{15}=N double bond is excluded [14].

3.2. Many Body Green's Function Theory

The MBGFT calculations in the QM/MM framework were carried out by interfacing the plane waves Yambo code [35] with the

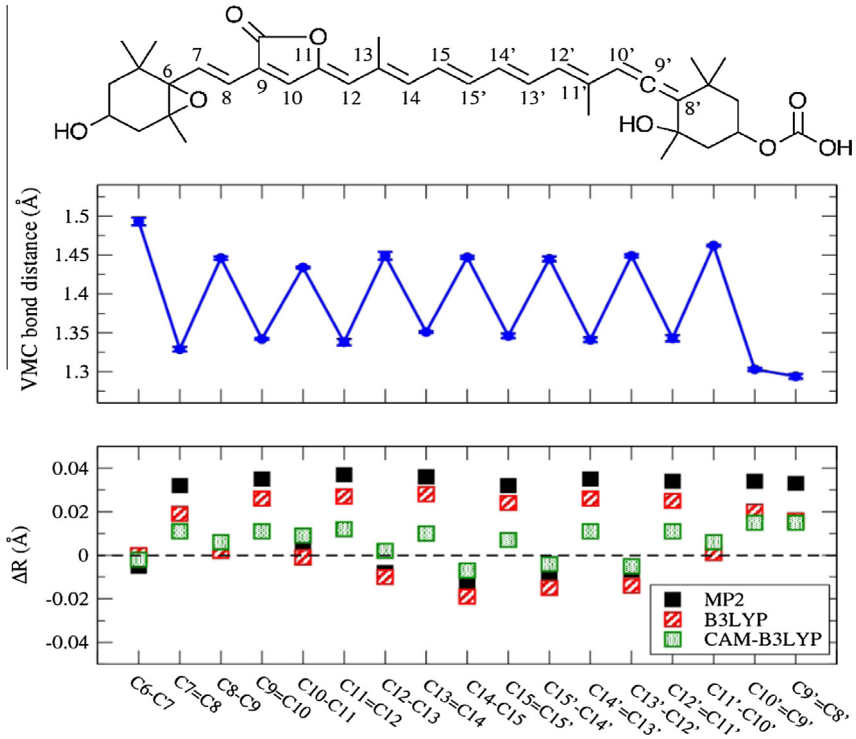

Fig. 2. PID: sketch representation of the chromophore, VMC BLA pattern for the gas phase molecule and differences with respect to other optimized structures (the reference is given by the VMC geometry). The average BLA for the VMC structure is 0.1165(10) Å [6] (the definition of the average BLA excludes $C_{9'}$=$C_{8'}$).

CPMD package [45]. The ground state electronic structure (Kohn–Sham eigenvalues and eigenvectors) have been calculated in a QM/MM scheme by CPMD and these quantities have been then used to calculate the self-energy corrections, and to build up the excitonic matrix, by the Yambo code. The gas phase excited states calculations have been also performed using the Yambo code, starting from the ground state electronic structure calculated by the Quantum Espresso package [58].

For both QM/MM and gas-phase calculations, Troullier–Martins norm-conserving pseudo-potentials [59] have been used with a plane-wave cutoff of 50 Ry.

The spurious interactions between images coming from periodic boundary conditions have been avoided by truncating the long range Coulomb interaction using the cutoff technique described in Ref. [60].

The self-energy expression, as well as the excitonic hamiltonian in plane wave formulation can be found in Ref. [35]. For the G^0W^0 correction 1500 states have been included to calculate the dynamical dielectric matrix $\epsilon_{G,G'}(\omega)$ (1.5 Ha cutoff) and the Green's function. For the BS spectra, we have included electron–hole pairs considering all the occupied and 100 unoccupied states. 1500 states have instead been included in the static polarization function. We have used a cutoff of 1.5 Ha for the screened interaction and of 20 Ha for the exchange component. After solving the BS equation by diagonalizing the excitonic Hamiltonian, the absorption spectra have been calculated by Eq. (11) by averaging the macroscopic dielectric function over the three Cartesian directions.

4. Results and discussion

In this section we report the main results obtained by the joint application of the VMC/MBGFT method for the **PID** and **RPSB** chromophore. While for the **PID** carotenoid we have considered until now only the structure and optical fingerprint in gas phase, for the **RPSB** molecule we extend both methodologies to a QM/MM framework in order to study the effect of the protein environment on both the structure and the optical spectra. We stress here that the MBGFT method for the calculation of excited states in a QM/MM formalism has been used until now only for one indole molecule in water solution [36], while we report in this work results for a complex system as the retinal in its protein environment.

The first step to be tackled is given by the geometrical issue. Both chromophores, **PID** and **RPSB**, are characterized by a polyenic chain responsible for the bright excitation: the accurate estimation of the BLA pattern therefore represents a key point in our VMC/MBGFT combined study. The VMC structure of the ground state of gas phase model of **PID** has been recently published by some of us [6]. VMC structures of **RPSB**, either in gas phase and in the protein environment, have been previously reported in a recent work by some of us [14]. One of the main goals of these previous works was to demonstrate the feasibility to obtain by VMC fully *ab initio* structures of large size chromophores such as **PID** and **RPSB**.

4.1. Gas phase *PID*

The VMC BLA pattern of **PID** [6] and the comparison between VMC and MP2//cc-pVDZ [61], B3LYP//6-31++G** and CAM-B3LYP//cc-pVDZ [6] data are respectively reported in the middle and at the bottom of Fig. 2. MP2 double bonds are seen to be systematically larger by 0.03–0.04 Å than the corresponding VMC bonds, whereas the single bonds are only slightly elongated between C_{12}—C_{13} and $C_{13'}$—$C_{12'}$ and almost coincident with the VMC ones in the extremal regions of the polyenic chain of **PID**. A similar trend has been verified for the B3LYP structure: the increase in the double bond length is in this case about 0.02–0.03 Å, the central single bonds are somewhat longer than the MP2 ones. The CAM-B3LYP structure is the most similar to the VMC geometry in terms of BLA pattern, with the largest differences (0.015 Å) identified in the two double bonds of the allene group.

As shown in Ref. [6] even small differences in the bond length alternation significantly alter vertical excitation energies of **PID**, since the molecular orbitals involved in the low-lying region of the absorption spectrum are delocalized along the polyenic chain. TDDFT and GW/BS calculations on the structures relaxed at various level of theory have shown a considerable dependence of the transition energies on the value of the average BLA, and a good agreement using the VMC structure (2.62 eV) with respect to the experimental results (2.72 eV) has been found for the first bright B_u^+-like excitation [6].

4.2. *RPSB: from gas phase to rhodopsin*

The VMC/MBGFT combined technique has been used in the present work to characterize the low-lying singlet states of **RPSB**, in analogy with what has carried out using TDDFT on VMC geometries [14]. Starting from the VMC structures, we have calculated the vertical energies for S_1 and S_2 excited states and the shifts due to the coupling with the opsin environment. The **RPSB** is the chromophore in several light-detecting proteins belonging to the family of G-protein-coupled receptors [1,62]. In rhodopsin the photon absorption induces a fast (∼200 fs) and efficient (quantum yield of ∼0.65) isomerization of **RPSB** from the 11-*cis* to the all-trans structure, thus triggering the vision cycle [62].

The isomerization mechanism involves a $S_0 \rightarrow S_1$ conical intersection along a reaction coordinate mainly given by the torsion of the central double bond C_{11}=C_{12} [63–66]. The photoinduced isomerization is in competition with the thermally activated mechanism, whose specific properties have been recently illustrated by Olivucci and coworkers [67].

The essential role of the protein environment in the isomerization mechanism is revealed by femtosecond spectroscopy experiments [65] and by QM/MM calculations: [63–66,68] the **RPSB** dynamics is indeed much slower and less efficient in solution [69–71].

In the case of **RPSB**, the rhodopsin environment induces a blue shift to S_1 and S_2 low-lying states [14,37,72–78]. A further aspect to be pointed out for **RPSB** is the strong interaction between the counterion Glu113 and the terminal nitrogen atom.

Several key geometrical parameters such as the average value of BLA, the dihedral angle $\phi(C_5—C_6—C_7—C_8)$ involving the torsion of the β-ionone ring and the distortion from planarity in rhodopsin environment have been shown to be crucial in the tuning of the optical absorption [14,37,75–77,79–82].

As we have already noted elsewhere [14], the net effect of the protein environment on the **RPSB** BLA pattern is an increase of the average BLA value (see Fig. 3) which is due to a stronger localization of the π electrons along the carbon chain: this effect is mainly due to the electrostatic coupling between the electronic density of the chromophore and the external field given by the surrounding residues.

Also in the case of the **RPSB** gas phase model, the MP2//cc-pVDZ geometry [15] is characterized by a larger amount of dynamical correlation with respect to the VMC structure and consequently a larger value of the average BLA; the same occurs for the B3LYP//cc-pVDZ [15] functional, even though, at variance with the findings for **PID**, any specific trend can be clearly individuated when comparing the calculated MP2 and B3LYP differences. BLA patterns obtained at CAM-B3LYP//cc-pVDZ [14] and M06-2X//cc-pVDZ [83] are very close to the VMC one, with the only exception (ΔR = 0.02 Å) of the C_6—C_7 single bond.

A more systematic trend has been found when moving to the **RPSB** structure optimized in a QM/MM scheme: the CASSCF//6-31G* bond pattern [37] produces a larger value for the average BLA, evidence of a stronger electronic localization with respect to the VMC model, B3LYP//6-31G* calculations [77] instead produce the opposite result, with a smaller difference between single and double bonds.

The electronic structure of the **RPSB** in the VMC geometry is shown in Fig. 4 where the density of states of the molecule in gas phase (green solid line) and in the rhodopsin environment (blue dot-dashed line) are compared both at the LDA (top panel) and GW (bottom panel) level. The presence of the protein environment produces a widening of the electronic gap already in the LDA calculation (0.25 eV) and the effect is enhanced when looking at the quasi-particle gap calculated within the GW approximation (0.4 eV). The quasi-particle gap calculated in GW approximation (4.45 eV) is in very good agreement with previous calculations [31]. In order to single out the effect of the environment on the electronic and optical properties of **RPSB**, the density of states of **RPSB** calculated for the gas phase structure extracted by the VMC/MM geometry relaxation (Distorted, red dashed line) is plotted in the same figure. From Fig. 4 one can see that the inclusion of the geometrical effects induced by the rhodopsin has the opposite effect of gap reduction (0.14 eV at LDA and 0.16 eV at GW level). The values of the electronic gap and the quasiparticle gap for the three cases are summarized in Table 1.

The absorption spectra calculated at GW/BS level, for the gas phase, distorted structure and in rhodopsin environment are plotted in Fig. 5. The calculated gas phase excitation energies (S_1 = 2.19 eV, S_2 = 2.98 eV) are in a very good agreement with previous BS calculations [31] and with the experimental values [80]. Passing from the gas phase to the opsin environment, a blue shift in the absorption spectrum is found for both S_1 and S_2 states, corresponding to 0.39 and 0.49 eV, respectively, together with a reduction of the oscillator strength of the S_2 state. The absorption spectrum of the distorted geometry is red-shifted with respect to the gas phase geometry as already noticed in previous calculations at different levels of theory (see Table 2) confirming the role played by the electrostatic coupling with the environment in reproducing the experimentally observed blue shift. The excitation energies are reported in Table 1. From the solution of the BS equation we have also analyzed the electron–hole pairs participating in the S_1 and S_2 states: S_1 is characterized by a predominant HOMO → LUMO character (89%) for both the gas phase and the distorted geometry independently on the coupling with the environment. The S_2 excitation in gas phase has mainly HOMO − 1 → LUMO (77%) character with a small percentage (8%) of the HOMO → LUMO + 1 transition. The same character with slightly different weight in the transitions is also found in rhodopsin (HOMO − 1 → LUMO (81%) and HOMO - → LUMO + 1 (7%)) and in the distorted structure (HOMO − 1 → LUMO (81%) and HOMO → LUMO + 1 (5%)).

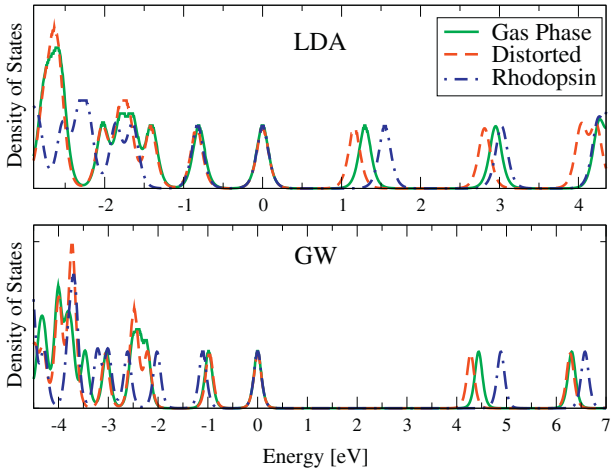

Fig. 4. Density of states for the gas phase **RPSB** (green solid line), the distorted geometry (red dashed-line) and in the protein environment (blue dashed-dot line), calculated at DFT (LDA) level (upper panel) and within G^0W^0 approximation (bottom panel). The zero energy has been set to the HOMO energy for all the structures in both approximations. (For interpretation of the references to color in this figure legend, the reader is referred to the web version of this article.)

Table 1
DFT (at LDA level), G^0W^0 gaps and vertical excitation energies (BS equation) for the S_1 and S_2 states for the **RPSB** in gas-phase, distorted geometry and in rhodopsin environment.

	DFT gap (eV)	G^0W^0 gap (eV)	Excitation energies (BS) (eV)
Gas phase	1.30	4.45	2.19, 2.98
Rhodopsin	1.55	4.85	2.58, 3.47
Distorted	1.16	4.30	2.03, 2.82

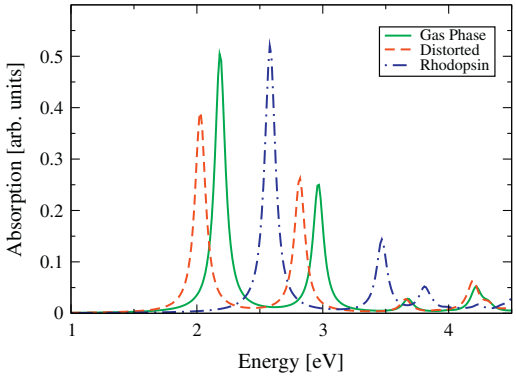

Fig. 5. Absorption spectra calculated solving the BS equation for **RPSB** in gas phase (green solid line), the distorted geometry (red dashed-line) and in the protein environment (blue dashed-dot line). Calculations include resonant-antiresonant coupling, the resulting spectra are obtained by averaging the photo-absorption cross section for light polarized along the three cartesian directions. An artificial broadening of 0.05 eV has been adopted. (For interpretation of the references to color in this figure legend, the reader is referred to the web version of this article.)

In the last decade a large number of theoretical investigations with different levels of sophistication has attempted to consistently characterize the bright excitation of 11-*cis* isomer of **RPSB**, as shown in Table 2, where a collection of computational results on **RPSB** is presented together with the experimental references. The choice of a specific technique for performing the geometry optimization and the theory used for the excited states calculations obviously turns to be crucial for an accurate determination of the optical fingerprint. Moreover, the size of the QM subsystem (beyond the full chromophore and including water molecules and some residues [76,84,87]) could have a sizable effect in the spectral tuning, as well as the use of a specific set of MM coordinates (X-ray or coming from a DFT annealing [14]) and force field.

In particular, we would stress the good agreement found between our VMC/MBGFT excitation energies and the very recent results obtained by using large-scale DFT calculations coupled with the frozen density embedding theory (FDET) approach by Zhou et al. [87]. The vertical energies in Ref. [87] have been calculated within the TDDFT framework taking into account 329 and 370 atoms in two different protein models. The overall FDET/TDDFT blue shift induced by the environment (0.27 eV, with respect to the gas phase optimized model) well matches with the VMC/MBGFT value of 0.39 eV: similarly, the effect of the electrostatic coupling with the surrounding residues corresponds to

Table 2
Present VMC/MBGFT results compared with a representative collection of theoretical and experimental data on **RPSB**.

S_0 geometry	S_1 excitation	Ref.	Gas phase	Distorted	Rhodopsin
VMC	MBGFT	this work	2.19	2.03	2.58
VMC	TD-B3LYP	[14]	2.26	2.05	2.54
DFT/B3LYP	TD-B3LYP	[84]	2.25	2.18	2.53
DFT/B3LYP	TD-B3LYP	[85]	–	–	2.58
DFT/PBE0	MCQDPT2	[76]	2.07	2.01	2.41
DFT/B3LYP	DMC	[15]	2.41(3)	–	–
DFT/B3LYP	DMC	[83]	2.37(3)	–	–
DFT/B3LYP	TD-B3LYP	[77]	–	–	2.46
DFT/B3LYP	MRCISD + Q	[78]	2.06	–	2.48
DFT/B3LYP	SAC-CI	[86]	–	–	2.45
DFT/M06-2X	CASPT2/S-IPEA	[83]	2.30	–	–
DFT/M06-2X	NEVPT2/SC	[83]	2.33	–	–
DFT/B3LYP (BP86)	FDET/TD-B3LYP	[87]	2.27	2.09	2.54
MP2	CASPT2/S-IPEA	[83]	2.24	–	–
MP2	NEVPT2/SC	[83]	2.27	–	–
MP2	CASPT2	[81]	2.05	–	–
CASSCF	CASPT2/0-IPEA	[88]	–	–	2.59
CASSCF	CASPT2/0-IPEA	[89]	2.28	–	–
CASSCF	CASPT2/0-IPEA	[80]	2.27	–	–
CASSCF	CASPT2/0-IPEA	[37]	–	2.18	2.50
CASSCF	CASPT2/0-IPEA	[75]	–	–	2.59
SCC-DFTB	CASPT2	[90]	–	1.93	2.47
	Expt.	[80]	2.03–2.34	–	–
	Expt.	[72–74]	–	–	2.48

0.45 eV for FDET/TDDFT and to 0.55 eV for VMC/MBGFT, indicating that our strategy based on fully *ab initio* methods and on QM subsystem coinciding with the full chromophore (54 atoms) produces a reliable description of the spectral tuning in rhodopsin. Within the same QM/MM approach, we also note that VMC/TDDFT (using B3LYP) results [14] are in remarkable agreement with the FDET/TDDFT findings.

5. Conclusions

We provide in this work a clear demonstration of the reliability of the *ab initio* combined VMC/MBGFT procedure to calculate vertical excited state energies of chromophores of biological relevance. We are able to perform geometry optimization at VMC level including the electrostatic and steric effects of the external, complex protein environment. Our recent works on the ground state geometry of **PID** and **RPSB** have shown the differences in terms of BLA pattern among several levels of theory, pointing out that the necessity to have a balanced description of dynamical correlation in order to obtain the correct ground state geometry.

MBGFT approach is well suited for the characterization of optical features of bulk and molecular systems. Our implementation of an interface between the MBGFT core and a QM/MM molecular dynamics package allowed us to apply MBGFT on a partition of the overall system, like a chromophore inserted in its protein binding pocket. Thanks to the abundance of theoretical and experimental data available in literature, the study of **RPSB** can represent a good benchmark to test the VMC/MBGFT computational protocol: our results on S_1 and S_2 low-lying excitation energies well reproduce the photophysics of **RPSB**, being in very good agreement with the best theoretical findings. In particular, the use of GW/Bethe–Salpeter approach in presence of the protein field is, to the best of our knowledge, the first attempt to calculate excitation energies of molecules of biological interest in their natural environment at MBGFT level.

In conclusion, VMC/MBGFT calculations within a QM/MM framework can be considered a valid tool to explore by first principles the absorption properties of organic dyes and biological chromophores in situ.

Acknowledgments

The European Research Council Project MultiscaleChemBio (No. 240624) within the VII Framework Program of the European Union has supported this work. The authors acknowledge Prof. Sandro Sorella for the assistance in the use of the TurboRVB Quantum Monte Carlo code. DV acknowledge also support from Futuro in Ricerca Grant No. RBFR12SW0J of the Italian Ministry of Education, University and Research, and European Community through the CRONOS project, Grant Agreement No. 280879. Computational resources were provided by the PRACE Consortium (Project PRA053), CINECA Computing Center and the Caliban-HPC Lab of the University of L'Aquila. The authors also acknowledge support from the EC's FP7 Grant No. 211956 (ETSF user project 211).

References

[1] O.P. Ernst, D.T. Lodowski, M. Elstner, P. Hegemann, L.S. Brown, H. Kandori, Microbial and animal rhodopsins: Structures, functions, and molecular mechanisms, Chem. Rev. 114 (2014) 126–163.
[2] T. Polívka, H.A. Frank, Molecular factors controlling photosynthetic light harvesting by carotenoids, Acc. Chem. Res. 43 (2010) 1125–1134.
[3] R.E. Blankenship, Molecular Mechanisms of Photosynthesis, Wiley-Blackwell, 2002.
[4] S. Hosseinkhani, Molecular enigma of multicolor bioluminescence of firefly luciferase, Cell. Mol. Life Sci. 68 (2011) 1167–1182.
[5] O.B. Malcoğlu, A. Calzolari, R. Gebauer, D. Varsano, S. Baroni, Dielectric and thermal effects on the optical properties of natural dyes: a case study on solvated cyanin, J. Am. Chem. Soc. 133 (2011) 15425–15433.
[6] E. Coccia, D. Varsano, L. Guidoni, Ab initio geometry and bright excitation of carotenoids: Quantum Monte Carlo and Many Body Green's Function Theory calculations on peridinin, J. Chem. Theory Comput. 10 (2014) 501–506.
[7] P.A. Limacher, K.V. Mikkelsen, H.P. Lüthi, On the accurate calculation of polarizabilities and second hyperpolarizabilities of polyacetylene oligomer chains using the CAM-B3LYP density functional, J. Chem. Phys. 130 (2009) 194114–194117.
[8] S. Chabbal, D. Jacquemin, C. Adamo, H. Stoll, T. Leininger, Bond length alternation of conjugated oligomers: another step on the fifth rung of Perdew's ladder of functional, J. Chem. Phys. 133 (2010) 151104–151107.
[9] D. Jacquemin, C. Adamo, Bond length alternation of conjugated oligomers: wave function and DFT benchmarks, J. Chem. Theory Comput. 7 (2011) 369–376.
[10] B.L. Hammond, W.A. Lester Jr., P.J. Reynolds, Monte Carlo Methods in Ab-Initio Quantum Chemistry, World Scientific, 1994.
[11] W.M.C. Foulkes, L. Mitas, R.J. Needs, G. Rajagopal, Quantum Monte Carlo simulations of solids, Rev. Mod. Phys. 73 (2001) 33–83.

[12] B.M. Austin, D.Y. Zubarev, W.A.J. Lester, Quantum Monte Carlo and related approaches, Chem. Rev. 112 (2012) 263–288.
[13] E. Coccia, L. Guidoni, Quantum Monte Carlo study of the retinal minimal model $C_5H_6NH_2^+$, J. Comput. Chem. 33 (2012) 2332–2339.
[14] E. Coccia, D. Varsano, L. Guidoni, Protein field effect on the dark state of 11-cis retinal in rhodopsin by Quantum Monte Carlo/Molecular Mechanics, J. Chem. Theory Comput. 9 (2013) 8–12.
[15] O. Valsson, C. Filippi, Photoisomerization of model retinal chromophores: insight from Quantum Monte Carlo and multiconfigurational perturbation theory, J. Chem. Theory Comput. 6 (2010) 1275–1292.
[16] E. Runge, E.K.U. Gross, Density-functional theory for time-dependent systems, Phys. Rev. Lett. 52 (1984) 997–1000.
[17] M.E. Casida, C. Jamorski, K.C. Casida, D.R. Salahub, Molecular excitation energies to high-lying bound states from time-dependent density-functional response theory: characterization and correction of the time-dependent local density approximation ionization threshold, J. Chem. Phys. 108 (1998) 4439–4449.
[18] B.O. Roos, Advances in Chemical Physics; Ab Initio Methods in Quantum Chemistry-II, Wiley, Chichester, 1987.
[19] K. Andersson, P.-A. Malmqvist, B.O. Roos, A.J. Sadlej, K. Wolinski, Second-order perturbation theory with a CASSCF reference function, J. Phys. Chem. 94 (1990) 5483–5488.
[20] K. Andersson, P.-A. Malmqvist, B.O. Roos, Second-order perturbation theory with a complete active space self-consistent field reference function, J. Chem. Phys. 96 (1992) 1218–1226.
[21] C. Angeli, R. Cimiraglia, J.-P. Malrieu, *N*-electron valence state perturbation theory: a fast implementation of the strongly contracted variant, Chem. Phys. Lett. 350 (2001) 297–305.
[22] C. Angeli, R. Cimiraglia, S. Evangelisti, T. Leininger, J.-P. Malrieu, Introduction of n-electron valence states for multireference perturbation theory, J. Chem. Phys. 114 (2001) 10252–10264.
[23] C. Angeli, R. Cimiraglia, J.-P. Malrieu, n-electron valence state perturbation theory: a spinless formulation and an efficient implementation of the strongly contracted and of the partially contracted variants, J. Chem. Phys. 117 (2002) 9138–9153.
[24] J.A. Pople, R. Seeger, R. Krishnan, Variational configuration interaction methods and comparison with perturbation theory, Int. J. Quantum Chem. Suppl. (1977) 149–163. Y-11.
[25] S. Grimme, M. Waletzke, A combination of Kohn–Sham density functional theory and multi-reference configuration interaction methods, J. Chem. Phys. 111 (1999) 5645–5655.
[26] M. Kleinschmidt, C.M. Marian, Waletzke, S. Grimme, Parallel multireference configuration interaction calculations on mini-β-carotenes and β-carotene, J. Chem. Phys. 130 (2009) 044708–044711.
[27] A. Szabo, N.S. Ostlund, Modern Quantum Chemistry, Dover Publications, 1996.
[28] C. König, A. Neugebauer, Quantum chemical description of absorption properties and excited-state processes in photosynthetic systems, ChemPhysChem 13 (2012) 386–425.
[29] G. Onida, L. Reining, A. Rubio, Electronic excitations: density-functional versus many-body Green's-function approaches, Rev. Mod. Phys. 74 (2002) 601–659.
[30] D. Varsano, A. Marini, A. Rubio, Optical saturation driven by exciton confinement in molecular chains: a time-dependent density-functional theory approach, Phys. Rev. Lett. 101 (2008) 133002.
[31] Y. Ma, M. Rohlfing, C. Molteni, Excited states of biological chromophores studied using many-body perturbation theory: effects of resonant-antiresonant coupling and dynamical screening, Phys. Rev. B 80 (2009). 241405(R)-4.
[32] Y. Ma, M. Rohlfing, C. Molteni, Modeling the excited states of biological chromophores within many-body Green's Function Theory, J. Chem. Theory Comput. 6 (2010) 257–265.
[33] C. Faber, P. Boulanger, I. Duchemin, C. Attaccalite, X. Blase, Many-body Green's function GW and Bethe–Salpeter study of the optical excitations in a paradigmatic model dipeptide, J. Chem. Phys. 139 (2013) 194308–194310.
[34] P. Boulanger, D. Jacquemin, I. Duchemin, X. Blase, Fast and accurate electronic excitations in cyanines with the many-body Bethe–Salpeter approach, J. Chem. Theory Comput. 10 (2014) 1212–1218.
[35] A. Marini, C. Hogan, M. Grüning, D. Varsano, Yambo: an ab initio tool for excited state calculations, Comput. Phys. Commun. 180 (2009) 1392–1403.
[36] A.M. Conte, E. Ippoliti, R.D. Sole, P. Carloni, O. Pulci, Many-body perturbation theory extended to the Quantum Mechanics/Molecular Mechanics Approach: application to indole in water solution, J. Chem. Theory Comput. 5 (2009) 1822–1828.
[37] G. Tomasello, G. Olaso-Gonzalez, P. Altoé, M. Stenta, L. Serrano-Andres, M. Merchan, G. Orlandi, A. Bottoni, M. Garavelli, Electrostatic control of the photoisomerization efficiency and optical properties in visual pigments: on the role of counterion quenching, J. Am. Chem. Soc. 131 (2009) 5172–5186.
[38] C.J. Umrigar, Two aspects of quantum Monte Carlo: determination of accurate wavefunctions and determination of potential energy surfaces of molecules, Int. J. Quantum Chem. 36 (1989) 217–230.
[39] S. Sorella, L. Capriotti, Algorithmic differentiation and the calculation of forces by quantum Monte Carlo, J. Chem. Phys. 133 (2010). 234111-10.
[40] M. Barborini, S. Sorella, L. Guidoni, Structural optimization by Quantum Monte Carlo: investigating the low-lying excited states of ethylene, J. Chem. Theory Comput. 8 (2012) 1260–1269.
[41] C. Attaccalite, S. Sorella, Stable liquid hydrogen at high pressure by a novel ab initio molecular-dynamics calculation, Phys. Rev. Lett. 100 (2008). 114501-4.
[42] A. Zen, Y. Luo, S. Sorella, L. Guidoni, Molecular properties by Quantum Monte Carlo: an investigation on the role of the wave function ansatz and the basis set in the water molecule, J. Chem. Theory Comput. 9 (2013) 4332–4350.
[43] S. Sorella, TurboRVB Quantum Monte Carlo package, 2013. <http://people.sissa.it/sorella/web/index.html> (accessed date: 17 December).
[44] A. Laio, J. VandeVondele, U. Röthlisberger, A Hamiltonian electrostatic coupling scheme for hybrid Car–Parrinello molecular dynamics simulations, J. Chem. Phys. 116 (2002) 6941–6947.
[45] CPMD, 2013, copyright IBM Corp 1990–2008, Copyright MPI für Festkörperforschung Stuttgart 1997–2001. <http://www.cpmd.org/> (accessed date: 10 November).
[46] M. Casula, S. Sorella, Geminal wave functions with Jastrow correlation: a first application to atoms, J. Chem. Phys. 119 (2003) 6500–6511.
[47] M. Casula, C. Attaccalite, S. Sorella, Correlated geminal wave function for molecules: an efficient resonating valence bond approach, J. Chem. Phys. 121 (2004) 7110–7126.
[48] L. Stella, C. Attaccalite, S. Sorella, A. Rubio, Strong electronic correlation in the hydrogen chain: a variational Monte Carlo study, Phys. Rev. B 84 (2011) 245117.
[49] E. Neuscamman, Size consistency error in the antisymmetric geminal power wave function can be completely removed, Phys. Rev. Lett. 109 (2012). 203001-5.
[50] E. Neuscamman, Communication: a Jastrow factor coupled cluster theory for weak and strong electron correlation, J. Chem. Phys. 139 (2013) 181101.
[51] E. Neuscamman, The Jastrow antisymmetric geminal power in Hilbert space: theory, benchmarking, and application to a novel transition state, J. Chem. Phys. 139 (2013) 194105.
[52] A. Zen, E. Coccia, Y. Luo, S. Sorella, L. Guidoni, Static and dynamical correlation in diradical molecules by Quantum Monte Carlo using the jastrow antisymmetrized geminal power ansatz, J. Chem. Theory Comput. 10 (2014) 1048–1061.
[53] R.W. Godby, R.J. Needs, Metal-insulator transition in Kohn–Sham theory and quasiparticle theory, Phys. Rev. Lett. 62 (1989) 1169–1172.
[54] M. Gruning, A. Marini, X. Gonze, Exciton-plasmon states in nanoscale materials: breakdown of the Tamm–Dancoff approximation, Nano Lett. 9 (2009) 2820–2824.
[55] S. Albrecht, L. Reining, R. Del Sole, G. Onida, Ab initio calculation of excitonic effects in the optical spectra of semiconductors, Phys. Rev. Lett. 80 (1998) 4510–4513.
[56] T.K. Woo, L. Cavallo, T. Ziegler, Implementation of the IMOMM methodology for performing combined QM/MM molecular dynamics simulations and frequency calculations, Theor. Chem. Acc. 100 (1998) 307–313.
[57] D.C. Teller, T. Okada, C.A. Behnke, K. Palczewski, R.E. Stenkamp, Advances in determination of a high-resolution three-dimensional structure of rhodopsin, a model of G-Protein-Coupled Receptors (GPCRs), Biochemistry 40 (2001) 7761–7772.
[58] P. Giannozzi, S. Baroni, N. Bonini, M. Calandra, R. Car, C. Cavazzoni, D. Ceresoli, G.L. Chiarotti, M. Cococcioni, I. Dabo, A. Dal Corso, S. de Gironcoli, S. Fabris, G. Fratesi, R. Gebauer, U. Gerstmann, C. Gougoussis, A. Kokalj, M. Lazzeri, L. Martin-Samos, N. Marzari, F. Mauri, R. Mazzarello, S. Paolini, A. Pasquarello, L. Paulatto, C. Sbraccia, S. Scandolo, G. Sclauzero, A.P. Seitsonen, A. Smogunov, P. Umari, R.M. Wentzcovitch, QUANTUM ESPRESSO: a modular and open-source software project for quantum simulations of materials, J. Phys.: Condensed Mat. 21 (2009) 395502–395519.
[59] N. Troullier, J.L. Martins, Efficient pseudopotentials for plane-wave calculations, Phys. Rev. B 43 (1991) 1993–2006.
[60] C.A. Rozzi, D. Varsano, A. Marini, E.K.U. Gross, A. Rubio, Exact coulomb cutoff technique for supercell calculations, Phys. Rev. B 73 (2006) 205119.
[61] S. Knecht, C.M. Marian, J. Kongsted, B. Mennucci, On the photophysics of carotenoids: a multireference DFT study of peridinin, J. Phys. Chem. B 117 (2013) 13808–13815.
[62] K. Palczewski, G protein-coupled receptor rhodopsin, Annu. Rev. Biochem. 75 (2006) 743–767.
[63] P.B. Coto, A. Sinicropi, L.D. Vico, N. Ferré, M. Olivucci, Characterization of the conical intersection of the visual pigment rhodopsin at the CASPT2//CASSCF/AMBER level of theory, Mol. Phys. 104 (2006) 983–991.
[64] L.M. Frutos, T. Andruniow, F. Santoro, N. Ferré, M. Olivucci, Tracking the excited-state time evolution of the visual pigment with multiconfigurational quantum chemistry, Proc. Nat. Acad. Sci. 104 (2007) 7764–7769.
[65] D. Polli, P. Altoé, O. Weingart, K.M. Spillane, C. Manzoni, D. Brida, G. Tomasello, G. Orlandi, P. Kukura, R.A. Mathies, M. Garavelli, G. Cerullo, Conical intersection dynamics of the primary photoisomerization event in vision, Nature 467 (2010) 440–443.
[66] I. Schapiro, M.N. Ryazantsev, L.M. Frutos, N. Ferré, R. Lindh, M. Olivucci, The ultrafast photoisomerizations of rhodopsin and bathorhodopsin are modulated by bond length alternation and HOOP driven electronic effects, J. Am. Chem. Soc. 133 (2011) 3354–3364.
[67] S. Gozem, I. Schapiro, N. Ferré, M. Olivucci, The molecular mechanism of thermal noise in rod receptors, Science 337 (2012) 1225–1228.
[68] O. Weingart, P. Altoé, M. Stenta, A. Bottoni, G. Orlandi, M. Garavelli, Product formation in rhodopsin by fast hydrogen motions, Phys. Chem. Chem. Phys. 13 (2011) 3645–3648.

[69] H. Kandori, Y. Katsuta, M. Ito, H.J. Sasabe, Femtosecond fluorescence study of the rhodopsin chromophore in solution, J. Am. Chem. Soc. 117 (1995) 2669–2670.
[70] R.S. Becker, K.J. Freedman, A comprehensive investigation of the mechanism and photophysics of isomerization of a protonated and unprotonated Schiff base of 11-cis-retinal, J. Am. Chem. Soc. 107 (1985) 1477–1485.
[71] J.E. Kim, M.J. Tauber, R.A. Mathies, Wavelength dependent cis-trans isomerization in vision, Biochemistry 40 (2001) 13774–13778.
[72] V.R. Rao, D.D. Oprian, Activating mutations of rhodopsin and other G protein-coupled receptors, Annu. Rev. Biophys. Biomol. Struct. 25 (1996) 287–314.
[73] T.P. Sakmar, S.T. Menon, E.P. Marin, A.E.S., RHODOPSIN: insights from recent structural studies, Annu. Rev. Biophys. Biomol. Struct. 31 (2002) 443–484.
[74] S. Filipek, R.E. Stenkamp, D.C. Teller, K. Palczewski, G protein-coupled receptor rhodopsin: a prospectus, Annu. Rev. Physiol. 65 (2003) 851–879.
[75] P.B. Coto, A. Strambi, N. Ferré, M. Olivucci, The color of rhodopsins at the ab initio multiconfigurational perturbation theory resolution, Proc. Nat. Acad. Sci. 103 (2006) 17154–17159.
[76] K. Bravaya, A. Bochenkova, A. Granovsky, A. Nemukhin, An opsin shift in rhodopsin: retinal S_0—S_1 excitation in protein, in solution, and in the gas phase, J. Am. Chem. Soc. 129 (2007) 13035–13042.
[77] A. Altun, S. Yokoyama, K. Morokuma, Spectral tuning in visual pigments: an ONIOM(QM:MM) study on bovine rhodopsin and its mutants, J. Phys. Chem. B 112 (2008) 6814–6827.
[78] A. Altun, S. Yokoyama, K. Morokuma, Mechanism of spectral tuning going from retinal in vacuo to bovine rhodopsin and its mutants: multireference ab initio quantum mechanics/molecular mechanics studies, J. Phys. Chem. B 112 (2008) 16883–16890.
[79] I.B. Nielsen, L. Lammich, L.H. Andersen, S_1 and S_2 excited states of gas-phase schiff-base retinal chromophores, Phys. Rev. Lett. 96 (2006). 018304-4.
[80] J. Rajput, D.B. Rahbek, L.H. Andersen, A. Hirshfeld, M. Sheves, P. Altoè, G. Orlandi, M. Garavelli, Probing and modeling the absorption of retinal protein chromophores in vacuo, Angew. Chem. Int. Ed. 49 (2010) 1790–1793.
[81] S. Sekharan, O. Weingart, V. Buss, Ground and excited states of retinal schiff base chromophores by multiconfigurational perturbation theory, Biophys. J.: Biophys. Lett. 91 (2006) L07–L09.
[82] I.V. Rostov, R.D. Amos, R. Kobayashi, G. Scalmani, M.J. Frisch, Studies of the ground and excited-state surfaces of the retinal chromophore using CAM-B3LYP, J. Phys. Chem. B 114 (2010) 5547–5555.
[83] O. Valsson, C. Angeli, C. Filippi, Excitation energies of retinal chromophores: critical role of the structural model, Phys. Chem. Chem. Phys. 14 (2012) 11015–11020.
[84] V.R.I. Kaila, R. Send, D. Sundholm, The effect of protein environment on photoexcitation properties of retinal, J. Phys. Chem. B 116 (2012) 2249–2258.
[85] J.A. Gascon, E.M. Sproviero, V.S. Batista, Computational studies of the primary phototransduction event in visual rhodopsin, Acc. Chem. Res. 39 (2006) 184–193.
[86] K. Fujimoto, S. Hayashi, J. Hasegawa, H. Nakatsuji, Theoretical studies on the color-tuning mechanism in retinal proteins, J. Chem. Theory Comput. 3 (2007) 605–618.
[87] X. Zhou, D. Sundholm, T.A. Wesolowski, V.R.I. Kaila, Spectral tuning of rhodopsin and visual cone pigments, J. Am. Chem. Soc. 136 (2014) 2723–2726.
[88] T. Andruniow, N. Ferré, M. Olivucci, Structure, initial excited-state relaxation, and energy storage of rhodopsin resolved at the multiconfigurational perturbation theory level, Proc. Nat. Acad. Sci. U.S.A. 101 (2004) 17908–17913.
[89] A. Cembran, R. Gonzalez-Luque, P.A.M. Merchan, F. Bernardi, M. Olivucci, M. Garavelli, Structure, spectroscopy, and spectral tuning of the gas-phase retinal chromophore: the β-ionone "handle" and alkyl group effect, J. Phys. Chem. A 109 (2005) 6597–6605.
[90] S. Sekharan, M. Suhigara, V. Buss, Origin of spectral tuning in rhodopsin – it is not the binding pocket, Angew. Chem. Int. Ed. 46 (2007) 269–271.